Fisher Information in the Moving-Mesh Reconstruction

Qiaoyin Pan,[1,2,*] Ue-Li Pen,[2,3,4,5,†] Derek Inman,[2,6] and Hao-Ran Yu[2,7]

[1]*School of Physics, Nankai University, 94 Weijin Rd, Nankai, Tianjin, 300071, China*
[2]*Canadian Institute for Theoretical Astrophysics, University of Toronto, 60 St. George Street, Toronto, Ontario M5S 3H8, Canada*
[3]*Dunlap Institute for Astronomy and Astrophysics, University of Toronto, Toronto, ON M5S 3H4, Canada*
[4]*Canadian Institute for Advanced Research, Program in Cosmology and Gravitation*
[5]*Perimeter Institute for Theoretical Physics, Waterloo, ON, N2L 2Y5, Canada*
[6]*Department of Physics, University of Toronto, 60 St. George, Toronto, ON M5S 1A7, Canada*
[7]*Kavli Institute for Astronomy and Astrophysics, Peking University, Beijing 100871, China*

(Dated: December 6, 2016)

Reconstruction techniques are commonly used in cosmology to reduce complicated nonlinear behaviour to a more tractable linearized system. We study the *Moving-Mesh* algorithm which is expected to perform better than many alternatives as it is based in Lagrangian space. To quantify the algorithm's ability to reconstruct linear modes, we study the Fisher information presented in 136 N-body simulations before and after reconstruction. We find that the linear scale is pushed to $k \simeq 0.3\ h/\mathrm{Mpc}$ after reconstruction. We furthermore find that the translinear plateau of the cumulative Fisher information is increased by a factor of ~ 40 after reconstruction, from $I \simeq 2.5 \times 10^{-5}/(\mathrm{Mpc}^3/h^3)$ to $I \simeq 10^{-3}/(\mathrm{Mpc}^3/h^3)$ at $k \simeq 1\ h/\mathrm{Mpc}$. This includes the decorrelation between initial and final fields, which has been neglected in many previous studies, and we find that the log-normal transform in this metric only gains a factor of 4 in information. We expect this technique to be beneficial to problems such as baryonic acoustic oscillations and cosmic neutrinos that rely on an accurate disentangling of nonlinear evolution from underlying linear effects.

PACS numbers:

I. INTRODUCTION

Two-point statistics provide a complete description of Gaussian density fields and can be computed efficiently even for large data sets. However, non-linear gravitational evolution leads to highly non-Gaussian matter distributions which require higher order statistics to fully characterize. Such statistics are computationally expensive and can be challenging to relate to cosmological parameters. To mitigate these difficulties, it is common to transform the matter field in a way that hopefully reduces non-Gaussianity. For example, Gaussianization transforms have been used to make the logarithmic distribution more Gaussian [1, 2] and Wavelet Non-Linear Wiener filters have been used to separate Gaussian and non-Gaussian components of the density field [3–5].

The success of techniques can be quantified by computing the Fisher information present in the power spectrum before and after reconstruction. For linear fields, the Fisher information is simply proportional to the number of modes (k^3). Rimes and Hamilton [6] were the first to study the Fisher information in the non-linear matter power spectrum calculated from N-body simulations. They found that the information has a plateau on translinear scales ($k \simeq 0.2 - 0.8\ h/\mathrm{Mpc}$) due to strong coupling of Fourier modes. Qualitatively, this means that the power spectrum on small scales gives little additional information. However, Harnois-Déraps et al. [5] computed the Fisher information for various Gaussianization methods (and combinations of methods) and found that while mode coupling is reduced, there is not necessarily an improvement in the cross correlation between the initial Gaussian density field and the final non-linear one.

In studies of Baryon Acoustic Oscillations (BAO), density fields are subjected to *reconstruction* which partially inverts non-linear evolution by applying a negative displacement field. This field is typically computed via Lagrangian perturbation theory (LPT) using the linear Zel'Dovich displacement, $-\nabla_q \cdot \mathbf{\Psi}(\boldsymbol{q})$ with respect to initial coordiantes $\boldsymbol{q}$ [7]. Recently, Zhu et al. [8] described how to use the Moving Mesh algorithm (MM), first described in [9, 10], to consistently compute $\mathbf{\Psi}(\boldsymbol{q})$ even for non-linear density fields. They further showed that even though shell-crossing and vorticity are not recovered, information is still recovered on scales relevent tot he BAO.

In this paper, we compute the Fisher information recovered after using this reconstruction scheme on 136 independent N-body simulations. The paper is organized as follows. In §II and III, we briefly describe the computation of the displacement potential using MM reconstruction and the N-body simulations used for the Fisher information computation. In §IV, we compute the power spectra, correlation matrix and Fisher information before and after reconstruction. Finally, in §V, we discuss the effectiveness of the reconstruction and its potential uses.

II. RECONSTRUCTION ALGORITHM

Detailed description of MM algorithm can be found in [11]. Here we quickly review it for completeness. The

*Electronic address: panda@mail.nankai.edu.cn
†Electronic address: pen@cita.utoronto.ca

aim of the reconstruction is to estimate the Lagrangian position, or the displacement, of particles from their final position only. Due to the highly nonlinear process at the late stage, it is hard to fully discrible the displacement field from the final condition. However, since the result in [12] showed that the E-mode displacement field has a strong correlation with the linear density field on large scale ($r > 0.5$ when $k \lesssim 2h/\mathrm{Mpc}$), estimating the E-mode displacement is expected to recover a large amount of information. It can be done by applying *Moving-Mesh* (MM) algorithm discribed in [11], which is originated from *Adapting Particle-Mesh* (APM) algorithm [9, 10].

The basic idea is to build a Particle-Mesh scheme on a curvilinear coordinate system, $\boldsymbol{\xi} = (\xi_1, \xi_2, \xi_3)$, in which number of particles per grid cell is set approximately constant. The displacement of particles in each grid cell is then approximately discribed by the deformation of the curvilinear grid on the Eulidean coordinate $\boldsymbol{x}(\boldsymbol{\xi}, t)$. Assuming that the deformation is a pure gradient, the physicsl position of particles on Eular coordinate is given as

$$x^i = \xi^\mu \delta^i_\mu + \Delta x^i, \tag{1}$$

where

$$\Delta x^i = \frac{\partial \phi}{\partial \xi^\nu} \delta^{i\nu}. \tag{2}$$

We use the convention the same as in [9], Latin indices denoting Cartesian coordinate, while Greek indices denoting the curvilinear grid coordinate. ϕ is called the deformation potential, and Δx^i the lattice displacement. The coordinate transfromation matrix $e^i_\mu = \partial x^i / \partial \xi^\mu$ is guarantee to be positive definite so that the volume element $\sqrt{g} \equiv \det \left| e^i_\mu \right|$ is always positive. This choice of the deformation can minimize the cell-crossing.

To solve the deformation potential ϕ, consider the continuity equation in curvilinear coordiante,

$$\frac{\partial (\sqrt{g}\rho)}{\partial t} + \partial_\mu \left[\rho \sqrt{g} e^\mu_i \left(v^i - \Delta \dot{x}^i \right) \right] = 0 \tag{3}$$

$\Delta \dot{x}^i = \delta^{i\nu} \partial_\nu \dot{\phi}$ is chosen such that the first term in Eq.3 is zero, resulting in a constant mass per volume element. The velocity field divergence is replaced by the deviation density field $\Delta \rho = \bar{\rho} - \rho\sqrt{g}$, which ideally should be zero. Then the deformation potential is described via the elliptic equation,

$$\partial_\mu (\rho \sqrt{g} e^\mu_i \delta^{i\nu} \partial_\nu \Delta \phi) = \Delta \rho. \tag{4}$$

The Eq.4 can be solved using multigrid algorithm described in [9, 10] (see also [11] for brief discription). The deformation Δx^i is closer to the displacement of particles when higher resolution is used to decribed the density field so that less particles are contained in each grid cell.

III. INPLEMENTATION

We use the CUBEP^{3}M [13] to run 136 simulations with a box size of 300 h^{-1}Mpc, afine resolution of 1024^3 cells and 512^3 totally particles. The initial conditions are computed using the transfer function given by CAMB [14] and then propogating the power linearly back to $z = 100$ with a growth factor. The Zel'dovich approximation is used to calculate the displacement and velocity fields, which are assigned to the particles. The cosmological parameters used are $\Omega_M = 0.32$, $\Omega_\Lambda = 0.679$, $h = 0.67$, $\sigma_8 = 0.83$, and $n_s = 0.96$. Different seeds are used to produce the initial conditions for different simulations so that they are independent to each other.

Then we run the MM reconstruction code on the nonlinear density fields from simulation in a resolution of ng = 128 per dimension. The multigrid algorithmis iterated for 1000 times in the result of the root mean square decreasing from ~ 4.5 to ~ 0.2. A 2D projection of one layer of the deformed grids and the original density field on the grid are given in Fig.1. As expected, there is no grid crossing after reconstruction.

IV. POWER SPECTRA AND INFORMATION CONTENT

The power spectrum is the Fourier transform of the correlation function and measures the amount of clustering in the matter distribution as a function of wavenumber k,

$$\langle \delta(\boldsymbol{k})\, \delta(\boldsymbol{k'}) \rangle = (2\pi)^3\, P(\boldsymbol{k})\, \hat{\delta}(\boldsymbol{k} - \boldsymbol{k'}), \tag{5}$$

where $\delta(\boldsymbol{k})$ is the density fluctuation in wave space, while $\hat{\delta}$ is the delta funciton. Of equal interest is $\Delta^2(k)$, the power spectrum in its dimensionless form, defined as

$$\Delta^2(k) \equiv \frac{k^3 P(k)}{2\pi^2}. \tag{6}$$

The power spectra of the mass distributions are calculated using the "*Nearest Grid Point*" (NGP) mass assignment scheme. In Fig.2(a) we plot the mean cross correlation function, $r = P_{\delta\delta_L} / \sqrt{P_\delta P_{\delta_L}}$ of the nonlinear and the linear power spectrum, and the reconstructed and linear power spectrum respectively. The wave number where the cross correlation drops to a half increases from $k \simeq 0.2\ h/\mathrm{Mpc}$ to $k \simeq 0.6\ h/\mathrm{Mpc}$ after the reconstruction. To qualify the improvement of cross correlation better, we compute the damping factors $\mathcal{D}(k) = r^4$ fitting the Gaussian BAO damping models $\mathcal{D}(k) = \exp(-k^2\Sigma^2/2)$. In Fig.2(a) we plot $\mathcal{D}_\delta^{1/4}$ ($\Sigma = 11.3$ Mpc/h) and $\mathcal{D}_{\delta_R}^{1/4}$ ($\Sigma = 3.9$ Mpc/h) over $r_{\delta\delta_L}$ and $r_{\delta_R\delta_L}$. We also plot $\mathcal{D}(k)^{1/4}$ that match cross correlation function after E-mode displacement reconstruction in [12] (ng = 512, box size = 400 Mpc/h, $\Sigma = 1.3$ Mpc/h), and MM reconstruction in a higer resolution in [11] (ng = 512, box size = 600 Mpc/h, $\Sigma = 2.6$ Mpc/h). We find that in higher resolution, the reconstruction gives a cross correlation damping at smaller scale. And it's expected that the E-mode displacement reconstruction gives a reconstructed power spectrum more correlated with the initial one, since it completely picks out the irrotational component of the real displacement field in N-body simulation, while through MM reconstruction, the difference

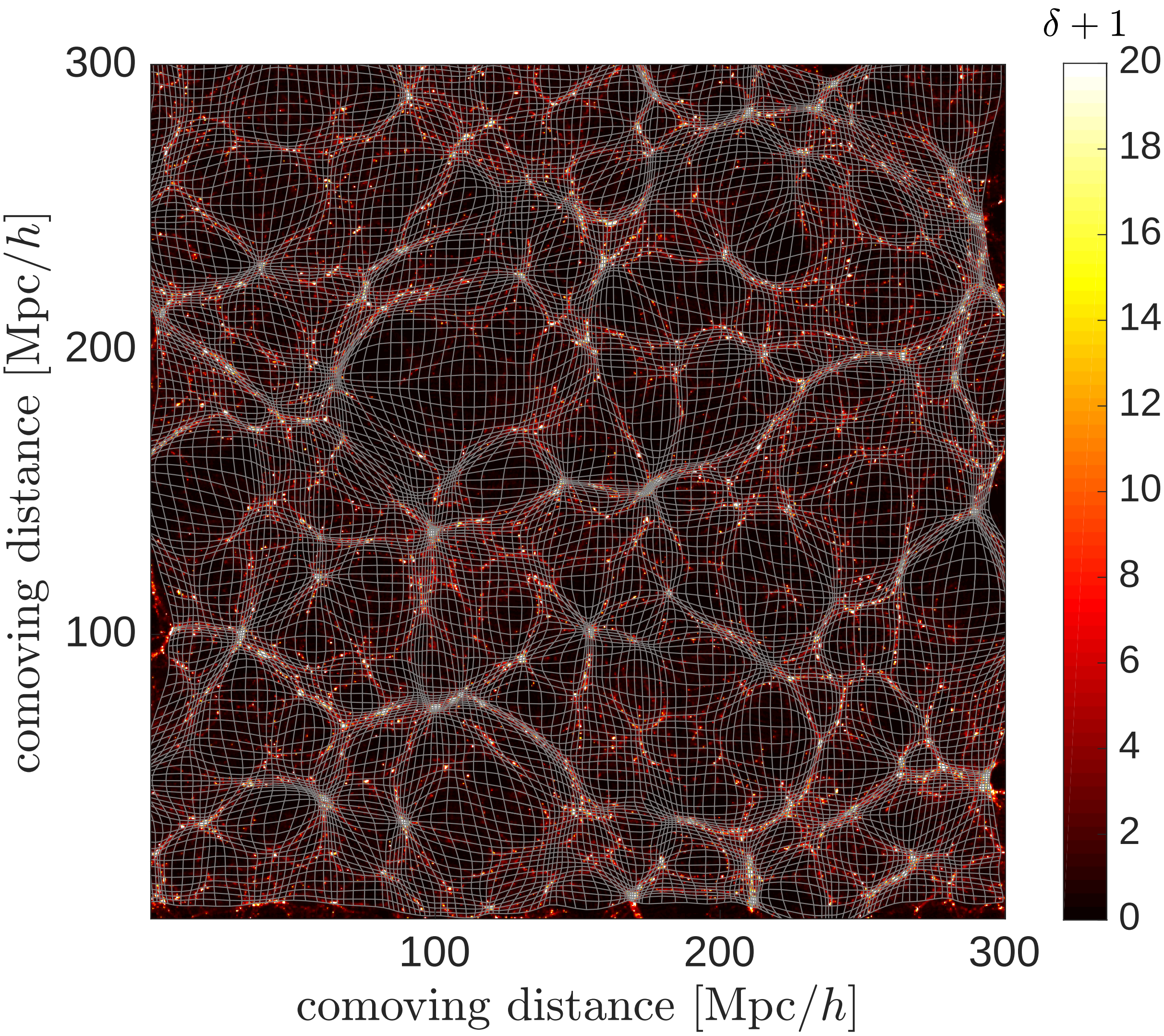

FIG. 1: The 2-D projection of the deformed grid of a sample N-body simulations is shown as curved white lines. The $\delta+1$ field on the deformed grid is shown underneath.

between the reconstructed displacement and the real displacement still contains an irrotational component, which is also correlated with the linear power spectrum. In Fig.2(b) we plot the linear power spectrum, and mean power spectrum (with error bars) of 136 nonlinear density fields and reconstrued density fields simply given by $\delta_R = -\nabla^2\phi$. The reconstructed power spectrum drops at nonlinear scale ($k \gtrsim 0.3\ h$/Mpc) since the reconstructed density fields are totally irrotational. The result is similar to that of E-mode displacement reconstruction described in [12], in which the reconstructed power spectrum drops, but in a different scale and at a different speed.

Mathamatically, the Fisher information [15] I in the log of amplitude A of the initial matter power spectrum is defined as

$$I_A \equiv -\left\langle \frac{\partial^2 \ln\mathcal{L}}{\partial A^2} \right\rangle, \tag{7}$$

in which $\mathcal{L}$ denotes the likelihood. For Gaussian fluctuations, the likelihood depends on parameters only through the power spectrum $P(k)$, so the information I in A defined by Eq.7 can be written as [6]

$$I_A = -\left\langle \sum_{k,k'} \frac{\partial \ln P(k)}{\partial \ln A} \frac{\partial^2 \ln\mathcal{L}}{\partial \ln P(k) \partial \ln P(k')} \frac{\partial \ln P(k')}{\partial \ln A} \right\rangle, \tag{8}$$

in which the angle bracket denotes the average over all the power spectra.

The definition Eq.8 can be written in a simpler form in two aspects, one of which is the first and the third partial dericative terms. For any density field δ, we can conveniently decompose it into linear and nonlinear components

$$\delta(k) = b(k)\delta_L(k) + n(k), \tag{9}$$

in which δ_L denotes the linear density field. $b(k)$ is the bias and $n(k)$ is defined such that the correlation $\langle \delta_L(k) n(k) \rangle$ is zero. If we correlate δ and δ_L,

$$\langle \delta(k)\delta_L(k) \rangle = b(k) \langle \delta_L(k)\delta_L(k) \rangle, \tag{10}$$

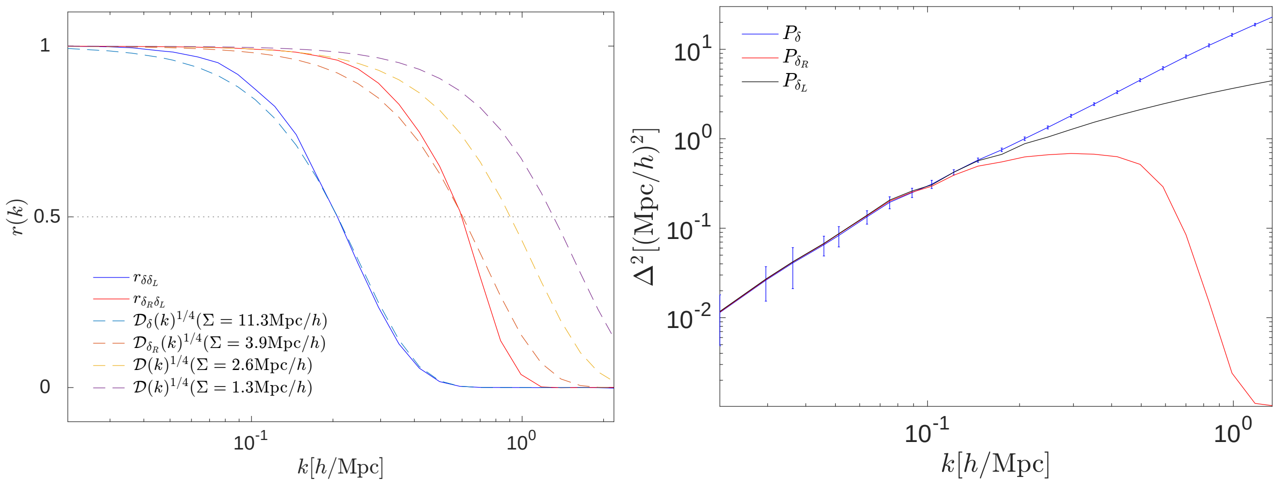

FIG. 2: (a) The cross correlation function (solid lines) $r_{\delta\delta_L}$ (blue) and $r_{\delta_R\delta_L}$ (red), and BAO damping models (dash lines). (b) The dimensionless power spectrum computed via linear theory (black), the mean value of 136 N-body simulations with 1σ error bars (blue), and reconstruction of the simulations (red).

we can solve for b as

$$b(k) = \frac{P_{\delta\delta_L}(k)}{P_{\delta_L}(k)}. \tag{11}$$

Non-linear evolution drives $b(k)$ to drop from unity, and generates the nonlinear term $n(k)$. Correlating δ and itself,

$$\langle \delta(k)\delta(k)\rangle = b^2(k)\langle \delta_L(k)\delta_L(k)\rangle + \langle n(k)n(k)\rangle, \tag{12}$$

we find

$$P_\delta(k) = \mathcal{D}(k)P_{\delta_L}(k) + P_n(k), \tag{13}$$

where $\mathcal{D}(k) \equiv b^2(k)$ is the nonlinear damping factor, and P_n is the mode coupling term.

With the help of Eq.11 and Eq.13, we can replace the partial derivatives $\partial \mathrm{ln}P(k)/\partial \mathrm{ln}A$ in Eq.8 with

$$\frac{A}{P(k)}\frac{\partial P(k)}{\partial A} = \frac{P^2_{\delta\delta_L}(k)}{P_\delta(k)P_{\delta_L}(k)}, \tag{14}$$

which is just the square of the cross correlation function $r^2(k)$, of δ and δ_L.

The second partial derivative terms in Eq.8, the Hessian of the vector $\mathrm{ln}P(k)$, has the expectation value of the Fisher matrix with respect to the log powers. For linear density fields, the Fisher matrix is approximately equal to the inverse of the covariance matrix of power spectrum estimates, which should be diagonal, with diagonal elements equal to number of modes in each wavenumber bin (when considering $\boldsymbol{k}$ and $-\boldsymbol{k}$ as the same mode). Thus we can write down a simpler matrix product form of cumulative Fisher information,

$$I_A\left(< k_n\right) = r^2(k)^{\mathrm{T}}\left[\mathrm{C}^{-1}_{\mathrm{norm}}(k,k')\right]r^2(k'), \tag{15}$$

where $\mathrm{C}_{\mathrm{norm}}$ is the normalized covariance matrix with size per dimension up to k_n, defined as

$$\mathrm{C}_{\mathrm{norm}}\left(k,k'\right) = \frac{\mathrm{Cov}(k,k')}{\langle P(k)\rangle\langle P(k')\rangle}, \tag{16}$$

and r is the mean cross correlation of a given density field with linear one as a function of k up to k_n. It's reliable to define Eq.15 for nonlinear density fields as well, since the Fisher matrix is approximately the same as that of linear density fields on linear scales. The covariance matrix is defined as

$$\mathrm{Cov}\left(k,k'\right) \equiv \frac{\sum_{i,j=1}^{N}\left[P_i\left(k\right) - \langle P\left(k\right)\rangle\right]\left[P_j\left(k'\right) - \langle P\left(k'\right)\rangle\right]}{N-1}, \tag{17}$$

where angle brackets mean the expected values, and N is the total number of simulations. The cross-correlation coefficient matrix, or for short the correlation matrix, is the normalized version of the covariance matrix,

$$\mathrm{Corr}\left(k,k'\right) = \frac{\mathrm{Cov}\left(k,k'\right)}{\sqrt{\mathrm{Cov}\left(k,k\right)\mathrm{Cov}\left(k',k'\right)}}, \tag{18}$$

which represents the correlation between different k modes. The corelation matrices for nonlinear and reconstructed power spectra are shown in Fig.3. For the nonlinear power spectra, the correlation matrix in the linear regime, $k \lesssim 0.07\ h/\mathrm{Mpc}$, is almost diagonal. The off-diagonal elements are produced by strong mode coupling in nonlinear scale, and the super-survey tidal effect which is small on linear scales but dominates in the weakly nonlinear regime [16]. The correlation matrix for the nonlinear power spectra has few negative elements ($\mathrm{Corr} \gtrsim -0.1$), which are produced by the unbiased error and thus will vanish with more simulations [17]. For the reconstructed correlation matrix, however, the linear regime expands up to $k \simeq 0.3\ h/\mathrm{Mpc}$, but number and magnitude of negative off-diagonal elements increases ($\mathrm{Corr} \gtrsim -0.8$).

Cumulative Fisher information is proportional to the volume. We plot the cumulative Fisher information per volume of the nonlinear, linear and reconstructed power specta in Fig.4(a). The Fisher information of the nonlinear power spectra drops from the linear one at $k \simeq$

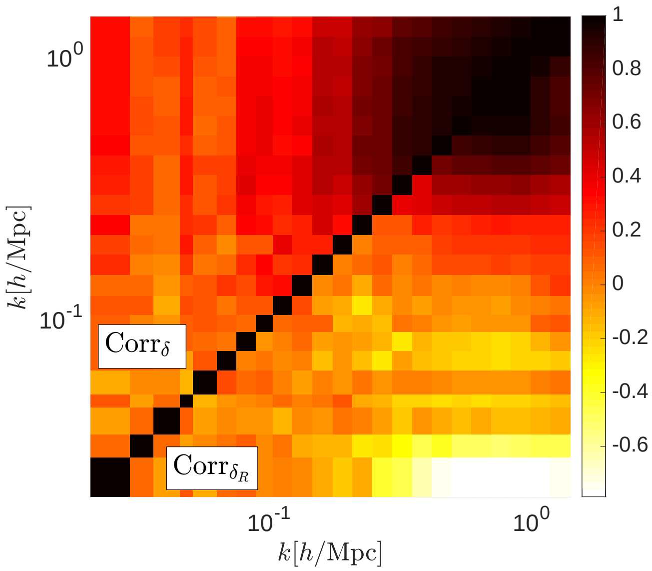

FIG. 3: Correlation coefficient matrix as found from 136 nonlinear power spectra (the upper-left elements) and the reconstructed power spectra (the lower-right off-diagonal elements). Both the matrix are symmetric and have unity diagonal elements.

0.05 h/Mpc, and has a flat plateau in the translinear regime, $k \simeq 0.3$ h/Mpc, with a saturated value of $I \simeq 2.5 \times 10^{-5}/(\mathrm{Mpc}^3/h^3)$. It indicates that there is nearly no independent information of the power spectrum in the translinear regime. But the information curve of the reconstructed power spectra keeps increasing roughly the same as the linear information until $k \simeq 0.3$ h/Mpc, and reaches its plateau at $k \simeq 0.8$ h/Mpc with the value of $I \simeq 10^{-3}/(\mathrm{Mpc}^3/h^3)$, up by a factor of 40. It indicates that the MM reconstructed method can strongly recover the lost information within this scale. We compare the Fisher information given by the MM reconstruction method with the logarithmic density mapping method [2] as an example to illustrate its strength. We find that the MM reconstruction gives more than 10 times more information than logarithmic mapping. In some papers, the cross correlation r^2 terms are set to be unity in Eq.15, which apparantly increases the nonlinear information. We also plot those in Fig.4(b) for better comparison. We find that, in this case, the nonlinear information drops from the linear one beginning at the same scale, $k \simeq 0.3$ h/Mpc, but reaches the saturated value, $I \simeq 4 \times 10^{-5}/(\mathrm{Mpc}^3/h^3)$, at translinear scale, $k \simeq 0.2 - 0.8$ h/Mpc. However, the MM reconstructed and logarithmic mapping information is higher than the linear one in the scale $k \simeq 0.2 - 0.5$ h/Mpc, which is not expected.

V. DISCUSSION AND CONCLUSION

The new reconstruction method successfully recovers the lost linear information on the mildly nonlinear scale, increasing the saturated information from $I \simeq 2.5 \times 10^{-5}/(\mathrm{Mpc}^3/h^3)$ to at least $I \simeq 10^{-3}/(\mathrm{Mpc}^3/h^3)$, and pushing the nonlinear scale to higher k. The result is better than previous methods (e.g. [2–4, 18]), and we believe that the reconstructed Fisher information will further increase to a greater magnitude in smaller scale since the cross correlation of the reconstructed power spectrum with the linear one increases in a higher resolution analysis [11]. The result in dark matter density fields gives a strong motivation to adapt the MM reconstruction to halo fields, neutrino fields, etc, so that we have access to the physics in smaller scales.

Reconstruction technique are concerned to improve cosmology measurements of BAO scale (e.g. [19, 20]). The successful application of the MM reconstruction on BAO reconstruction in 1D [8] and 3D [11] cosmology provide an intuitive view of the algorithm to push forward BAO research.

The MM reconstruction effectively decomposes the irrotational part and the curl part of the displacement field of particles. However, the reconstructed displacement might be greatly different from the real displacement in N-body simulation, since it is sensitive to the late stage shell-crossing and nonlinear process so that the original position of some spectific particles are replaced by each other. It is meaningful to compare the irrotational displacement field through the MM reocnstruction and through E-mode displacement reconstruction [12]. Since the MM reconstruction only needs the density field input and gives a large amount of recovering of lost information, it's expected to have a good effect on reconstructing the matter density field from observation.

Acknowledgments

We thank Hong-Ming Zhu,Yu Yu and Xin Wang for friendly and helpful discussions. Computations are performed on the General Purpose Cluster supercomputer at the SciNet HPC Consortium. SciNet is funded by: the Canadian Foundation for Innovation under the auspices of Compute Canada; the Government of Ontario; Ontario Research Fund - Research Excellence; and the University of Toronto.

[1] D. H. Weinberg, MNRAS **254**, 315 (1992).
[2] M. C. Neyrinck, I. Szapudi, and A. S. Szalay, ApJ **698**, L90 (2009), 0903.4693.
[3] T.-J. Zhang, H.-R. Yu, J. Harnois-Déraps, I. MacDonald, and U.-L. Pen, ApJ **728**, 35 (2011), 1008.3506.
[4] H.-R. Yu, J. Harnois-Déraps, T.-J. Zhang, and U.-L. Pen, MNRAS **421**, 832 (2012), 1012.0444.
[5] J. Harnois-Déraps, H.-R. Yu, T.-J. Zhang, and U.-L. Pen, MNRAS **436**, 759 (2013), 1205.4989.
[6] C. D. Rimes and A. J. S. Hamilton, MNRAS **360**, L82

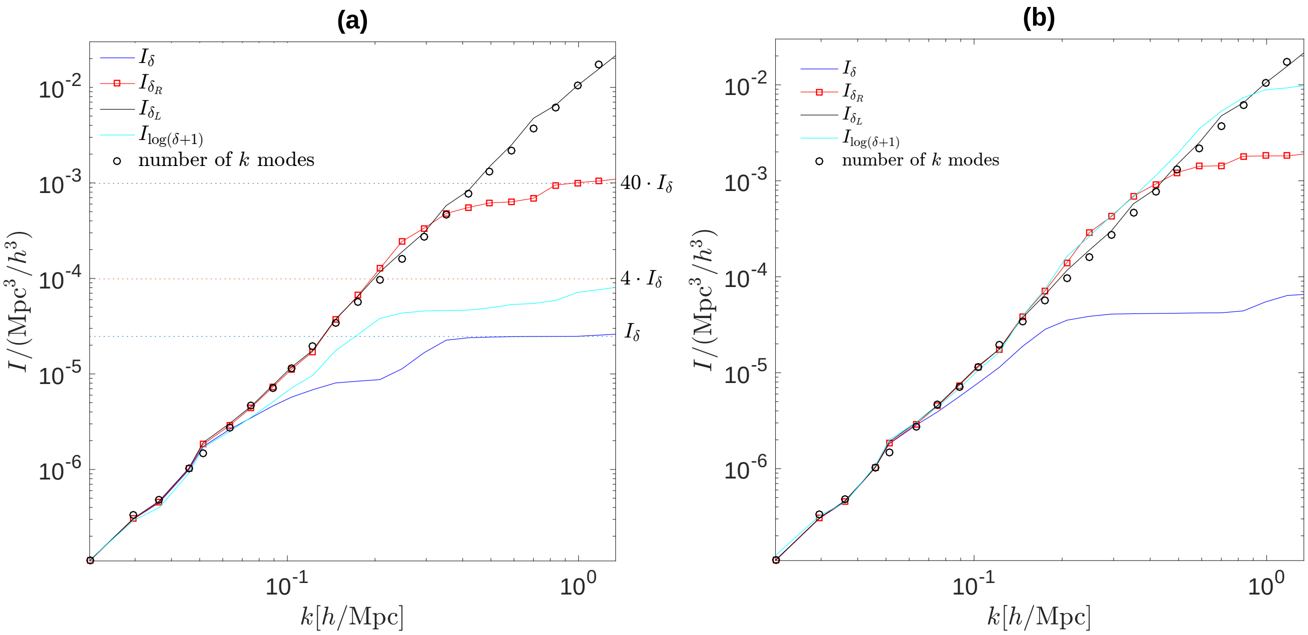

FIG. 4: (a) Cumulative Fisher information per volume in the power spectra as a function of wavenumber. The blue line corresponds to the nonlinear density fields; the red line with squares corresponds to the the reconstructed density fields; the dark line corresponds to the linear density fields; the circles correspond to number of k modes up to that wave bin. Dotted lines correspond to saturated value of nonlinear Fisher information, 4 times and 40 times of it, respectively. (b) Cumulative Fisher information per volume given by setting the cross correlation to be unity. The black, blue and cyan lines match the results in [2, 6].

(2005), astro-ph/0502081.

[7] Y. B. Zel'dovich, A&A **5**, 84 (1970).

[8] H.-M. Zhu, U.-L. Pen, and X. Chen, ArXiv e-prints (2016), 1609.07041.

[9] U.-L. Pen, ApJS **100**, 269 (1995).

[10] U.-L. Pen, ApJS **115**, 19 (1998), astro-ph/9704258.

[11] H.-M. Zhu, Y. Yu, U.-L. Pen, X. Chen, and H.-R. Yu (2016), 1611.09638.

[12] H.-R. Yu, U.-L. Pen, and H.-M. Zhu, ArXiv e-prints (2016), 1610.07112.

[13] J. Harnois-Déraps, U.-L. Pen, I. T. Iliev, H. Merz, J. D. Emberson, and V. Desjacques, MNRAS **436**, 540 (2013), 1208.5098.

[14] A. Lewis, A. Challinor, and A. Lasenby, ApJ **538**, 473 (2000), astro-ph/9911177.

[15] M. Tegmark, A. N. Taylor, and A. F. Heavens, ApJ **480**, 22 (1997), astro-ph/9603021.

[16] K. Akitsu, M. Takada, and Y. Li, ArXiv e-prints (2016), 1611.04723.

[17] R. Takahashi, N. Yoshida, M. Takada, T. Matsubara, N. Sugiyama, I. Kayo, A. J. Nishizawa, T. Nishimichi, S. Saito, and A. Taruya, ApJ **700**, 479 (2009), 0902.0371.

[18] M. C. Neyrinck, I. Szapudi, and C. D. Rimes, MNRAS **370**, L66 (2006), astro-ph/0604282.

[19] D. J. Eisenstein, H.-J. Seo, E. Sirko, and D. N. Spergel, ApJ **664**, 675 (2007), astro-ph/0604362.

[20] M. White, MNRAS **450**, 3822 (2015), 1504.03677.